Nonisothermal Bulk Crystallization Studies of High Density Polyethylene Using Light Depolarizing Microscopy

PITT SUPAPHOL, JOSEPH E. SPRUIELL

Center for Materials Processing; Department of Materials Science & Engineering, University of Tennessee, 434 Dougherty Engineering Bldg., Knoxville, Tennessee 37996-2200

Received 9 May 1997; revised 23 September 1997; accepted 25 September 1997

ABSTRACT: The quiescent nonisothermal bulk crystallization kinetics of two high-density polyethylene resins were investigated by a modified light-depolarizing microscopy (LDM) technique. The technique allows studies at average cooling rates up to 2500°C/min. The polymer was found to crystallize at a pseudo-isothermal temperature even at these very high cooling rates. The overall bulk crystallization rate increased rapidly as the cooling rate and supercooling increased. Crystallization kinetics was analyzed by Avrami analysis. Avrami exponents near 3 suggested spherical growth geometry and instantaneous nucleation at predetermined sites. Observation of spherulites by optical microscopy together with a number density of spherulites that changed little with increase in cooling rate or supercooling supported this model of crystallization behavior. Analysis of the half-time of crystallization based on the Lauritzen and Hoffman secondary nucleation theory indicated that the regime II-III transition was found to occur at a degree of supercooling of approximately 22°C. J Polym Sci B: Polym Phys **36:** 681–692, 1998

Keywords: high-density polyethylene; nonisothermal crystallization kinetics; plateau temperature; regime transition; crystallinity

INTRODUCTION

Isothermal crystallization of high-density polyethylene and other semicrystalline polymers has been studied extensively (e.g., refs. 1–5). These studies normally involve crystallization in a rather narrow temperature range and at relatively low amounts of supercooling due to limitations on the ability to establish controlled isothermal conditions outside of this range. However, polymer processing is normally carried out under nonisothermal conditions and at high degrees of supercooling. The present experiments were carried out in order to extend the range of experimental kinetics measurements, and to improve the understanding of the relationship between nonisothermal and isothermal kinetics.

Correspondence to: J. E. Spruiell

Journal of Polymer Science: Part B: Polymer Physics, Vol. 36, 681–692 (1998)
 CCC 0887-6266/98/040681-12

The technique used for the present studies was developed recently by Ding and Spruiell[6,7]; described in detail in ref. 7, it is based on the earlier work of Magill[8,9] who introduced the light-depolarizing microscopy technique as a method of investigating the overall kinetics of the crystallization process. The new technique allows for studies under nonisothermal conditions in the average cooling rate range of 5–2500°C/min. Basically, a thin sample is cooled by a constant temperature gas which is blown over it. The sample therefore does not cool at constant rate, but its cooling is analogous to that occurring in most polymer processing operations. The temperature of the sample is measured and recorded via the signal from a thermocouple embedded directly in the sample. These cooling conditions readily show that, prior to crystallization, the temperature of the sample is given by[7]:

$$T - T_s = (T_0 - T_s)\exp[-(\mathrm{CRF})t], \qquad (1)$$

where T, T_s, and T_0 are the temperature of the sample at arbitrary time t, of the cooling medium, and of the sample before starting to cool down, respectively. CRF is defined as the "cooling rate factor," and has units of reciprocal time (i.e., s^{-1}). It is a function of the sample volume, density, specific heat, and heat transfer coefficient at the sample/air interface. In this new technique, the value of CRF is used as a measure of the sample cooling condition. It is determined from the experimentally measured temperature versus time curves by fitting to eq. (1). It can also be related to the average cooling rate of the sample.

As discussed in ref. 7, the relative crystallinity, $\theta(t)$, can be obtained from the relative light intensity data according to the following formula:

$$\theta(t) = \frac{\chi_t}{\chi_\infty} = \frac{R - R_0}{R_\infty - R_0}, \quad (2)$$

where χ_t and χ_∞ are the absolute crystallinity at arbitrary time t and at infinite time; R, R_0, and R_∞ are the relative light intensities at arbitrary time t, at time zero and at infinite time, respectively. The relative light intensity is obtained from the ratio:

$$R = \frac{(I - C)}{I_0}, \quad (3)$$

where I and I_0 are the light intensities collected with and without an analyzer in the microscopy system. C is an empirical constant, related to the physical conditions of the technique, which is determined for each set of experiments. Use of the procedure defined by eqs. (2) and (3) to obtain the relative crystallinity corrects for light scattering from the many small spherulites existing in the early stages of crystallization; see ref. 7 for details.

For the present experiments, the relative crystallinity versus time data are analyzed, with ease and reliability, according to the Avrami eq. (10):

$$\theta(t) = 1 - \exp(-kt^n), \quad (4)$$

where k is the rate constant and n is the Avrami exponent.

Since, in this technique, the half-time of crystallization, $t_{1/2}$, defined as the time from the initiation of crystallization to the point where the relative crystallinity equals 50%, at different crystallization temperatures can be readily obtained, the data acquired can then be analyzed based on the secondary nucleation growth rate theory of Hoffman et al.[11] According to this theory, the linear growth rate, G, can be written as:

$$G = G_0 \exp\left[- \frac{U^*}{R(T_c - T_\infty)} \right] \exp\left[- \frac{K_g}{T_c(\Delta T)f} \right], \quad (5)$$

where G_0 is a preexponential term which is not strongly dependent on temperature. U^* is the activation energy of the elementary jump process which governs the mobility of the polymer with respect to the temperature and is commonly given by a universal value of 6276 J/mol,[11] T_c is the crystallization temperature, T_∞ is the WLF temperature at which the mobility of the molecules converges to zero and is frequently assumed to be $T_g - 30$, R is the gas constant, K_g is the nucleation exponent, ΔT is the degree of supercooling, and f is a factor used to correct for the temperature dependence of the heat of fusion.

At this point, there must be a connection between the half-time of crystallization and the linear growth rate in order to apply the secondary nucleation theory to the analysis of the crystallization regimes using the half-time data. This can be done based on the fact that the crystallization rate constant obtained experimentally from eq. (4) has a direct relationship with both the half-time of crystallization and the linear growth rate. If the polymer crystallizes with the spherulitic geometry and heterogeneous nucleation mode, such a relation can be formulated as:

$$(\ln 2)\left(\frac{1}{t_{1/2}}\right)^3 = \frac{4}{3}\pi G^3 N, \quad (6)$$

where N is the nucleation density.

Based on eqs. (5) and (6), the final relationship can then be written as:

$$\log(t_{1/2})^{-1} + \frac{U^*}{2.303R(T_c - T_\infty)} = A_2 - \frac{K_g}{2.303T_c(\Delta T)f'} \quad (7)$$

where A_2 is a combined constant. Finally, construction of $\log(t_{1/2})^{-1} + U^*/2.303R(T_c - T_\infty)$ ver-

sus $1/T_c(\Delta T)^m f^m$ serves as the regime test for instantaneous nucleation type, if $m = 1$, and for sporadic nucleation type, if $m = 2$.

EXPERIMENTAL

Materials

The HDPE materials were supplied by the Dow Chemical Company in the form of two different average molecular weight resins. The weight-average molecular weight of the as-received resins were 101,300 and 77,600 with polydispersities of 1.88 and 2.03, respectively. The higher molecular weight resin was labeled E12 while the lower molecular weight one was labeled E13. In order to eliminate possible variation in properties of the polymer from pellet to pellet, a large number of pellets was cut into pieces, mixed together, and then melt pressed at 160°C into film.

Nonisothermal Crystallization

Samples used in the LDM technique were prepared by cutting portions from the film made earlier. A 25.4 mm diameter, J-type iron/constantan thermocouple was placed between two portions of film, which were later sandwiched by a pair of clean glass slides. The whole setup was then transferred to a hot-stage, which was preset at 160°C and the sandwich was carefully pressed to give a sample of the desired thickness, which was controlled at 80 ± 1 μm. The sample was then placed in a special sample chamber, which was later secured on a microscope sample stage. Light of controlled intensity and noise was passed through the sample and into the objective lens. The eyepieces of the binocular microscope were replaced with photocells, which were set with and without analyzer. Heating of the sample was accomplished by passing nitrogen gas through a separate heating unit prior to impingement on the sample. Cool nitrogen gas replaced the hot nitrogen when the cooling process was begun. A personal computer was used to record the light intensity and temperature data simultaneously. A schematic of the equipment and a detailed description of it are given in ref. 7.

Average Spherulitic Size and Crystallinity Content

In order to investigate the average spherulitic size and crystallinity content as a function of the cooling rate, 10 samples from each resin were cooled down at different cooling rates in the range of 10–3,500°C/min. Small-angle light scattering (SALS) was used to measure the average spherulitic size of each sample prepared. After that, each sample was bisected and was later examined by two different techniques, density gradient column (DGC) and differential scanning calorimetry (DSC), for its crystallinity content.

Isopropanol and ethylene glycol were used to prepare a density gradient column providing the density range of 0.85–0.97 g/cm^3. Once, equilibrium of each sample which was put into the column was reached, the density of each sample was calculated from the equilibrium position, and later the absolute crystallinity content was obtained. A well-calibrated Perkin-Elmer DSC-7 was used to investigate thermal properties of the other half of each prepared sample. The sample weight was kept in the range of 3–4 mg in order to guarantee an optimal result. A heating rate of 20°C/min was used throughout all the runs. The absolute crystallinity content was calculated from the enthalpy of fusion obtained.

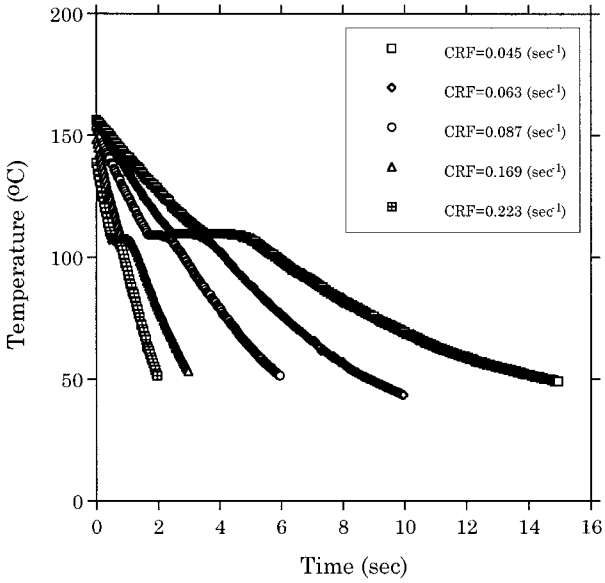

Figure 1. Cooling curves for E12 resin at various cooling rates.

RESULTS AND DISCUSSION

Nonisothermal Crystallization Kinetics

Figure 1 shows the actual cooling curves at five different values of CRF. For a particular cooling

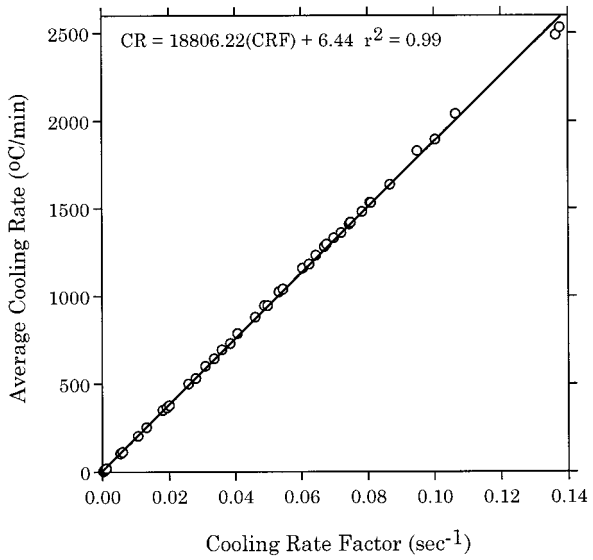

Figure 2. Experimental relationship between average cooling rate in °C/min and the cooling rate factor, CRF.

curve, it is obvious that the temperature drops drastically at the very beginning of the cooling process due to the large temperature difference between the cooling medium and the sample. The temperature continues to drop to the point where the crystallization process begins. Liberated heat associated with the crystallization process compensates for the heat taken away by the cooling medium, resulting in a constant temperature hold or "plateau" in the temperature profile. After the plateau, the temperature again continues to drop but at a slower rate due to the smaller temperature difference between the cooling medium and the sample. As will become clear below, the bulk of the crystallization occurs while the temperature is constant at the plateau temperature. Consequently, we will consider the plateau temperature and crystallization temperature to be synonymous. In addition, the presence of the plateau in the temperature profile has been previously observed in fiber melt-spinning process.[12,13]

Values of CRF (Fig. 1) were determined by fitting the region of the curves above the plateau to eq. (1). An "average cooling rate" (°C/s) was also determined by fitting the same portion of the curves to a linear equation. The relationship of the average cooling rate to the CRF is illustrated in Figure 2.

The plateau or crystallization temperature is directly related to the CRF, as illustrated in Figure 3. As mentioned earlier, the existence of the plateau is caused by the rate of heat liberation due to the crystallization process being the same as that taken away by the cooling medium. As the cooling rate increases, balance occurs at a lower temperature. This corresponds to a faster crystallization rate that is required to balance the rate of heat removal from the sample. Since the crystallization is occurring much faster, the time over which the plateau exists is much shorter.

The light intensities collected both with and without analyzer and the resulting relative light intensity curves are illustrated in Figure 4 for the E12 resin cooled at CRF = 0.005 s. In the molten state, prior to the onset of crystallization, both light intensities are constant, but it is obvious that the value of the light intensity collected with analyzer exhibits a much lower value due to the presence of the analyzer (with perfect, crossed polars and an isotropic sample, the intensity would be zero). As crystallization begins, the light collected without analyzer is scattered by the formation of numerous small spherulites, resulting in a substantial decrease in the transmitted light intensity. For the light intensity collected with the analyzer, the light scattered at the beginning of the crystallization process causes a small dip in the intensity data. The intensity data later increases as the light passing through the crystals is depolarized. The presence of an increase in light intensity collected without analyzer relates to a decrease in the light scattered due to increasing

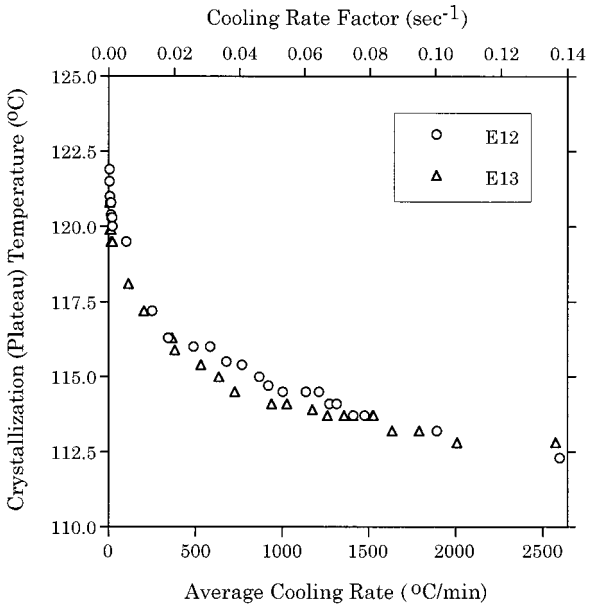

Figure 3. Typical plateau temperature versus average cooling rate and/or CRF.

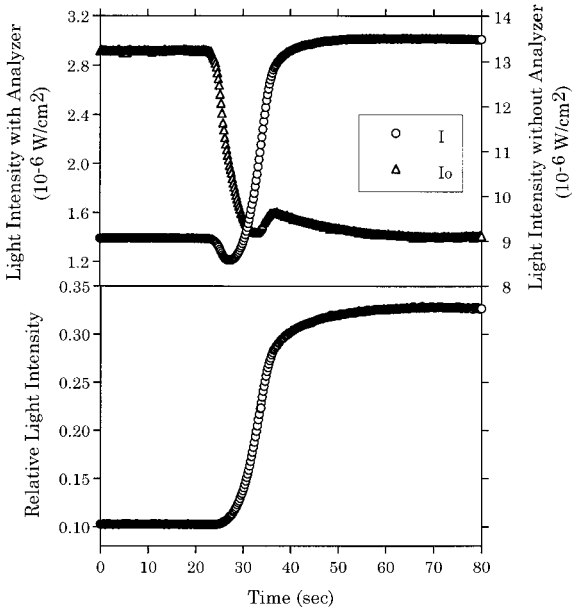

Figure 4. Typical light intensities both with and without analyzer and their resulting relative light intensity.

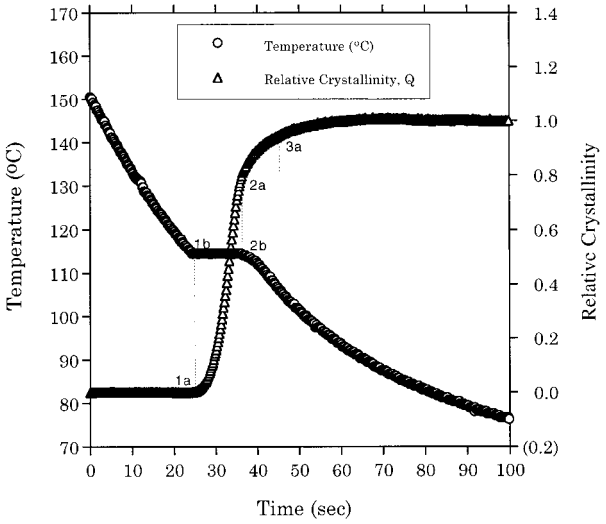

Figure 5. Overlay plot of temperature and relative crystallinity curves (data taken from E12 at CRF = 0.005 s).

spherulite size and to impingement of the crystal morphology. After impingement, changes in both light intensities were very slow due to internal changes in the crystal morphology which may be attributed to secondary crystallization. Calculation of the relative light intensity, R, provides the necessary correction for the effect of the light scattering and allows an accurate computation of the relative crystallinity via eq. (2).

An overlay plot of temperature and relative crystallinity curves for sample E12 with CRF = 0.005 s is presented in Figure 5. Points 1b and 2b stand for the starting and ending points for the plateau temperature. Points 1a and 2a represent the corresponding points on the relative crystallinity curve. It is clear that point 1a corresponds to the point at which the primary crystallization process has just gotten underway. The heat liberated by the crystallization process results in the onset of the plateau. After the crystallization process has started, the phase transformation from melt to solid proceeds very rapidly and at nearly constant temperature. According to video images recorded during the process, point 2a appears to coincide with the early stages of spherulite impingement; whereas, point 3a corresponds to the completion of impingement. Beyond point 3a, only secondary crystallization occurs, which involves the continued incorporation of amorphous chain segments into the existing crystals.

Figure 6 plots the relative crystallinity for five cooling rates of resin E12 against time. An induction period, defined as the time the sample spends going from its equilibrium melting temperature till the initiation of crystallization, decreases rapidly with increase in CRF. It should be noted that the parameters T_m^o for E12 and E13 resins were taken from the values on similar resins obtained by Kim[14] using SAXS: they are 142.7 and 141.3°C, respectively. Figure 7 shows the induction time,

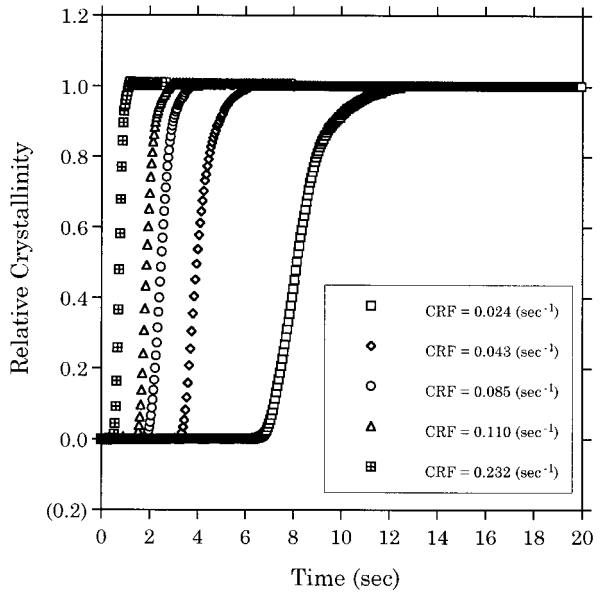

Figure 6. Relative crystallinity versus time at five cooling rates for E12 resin.

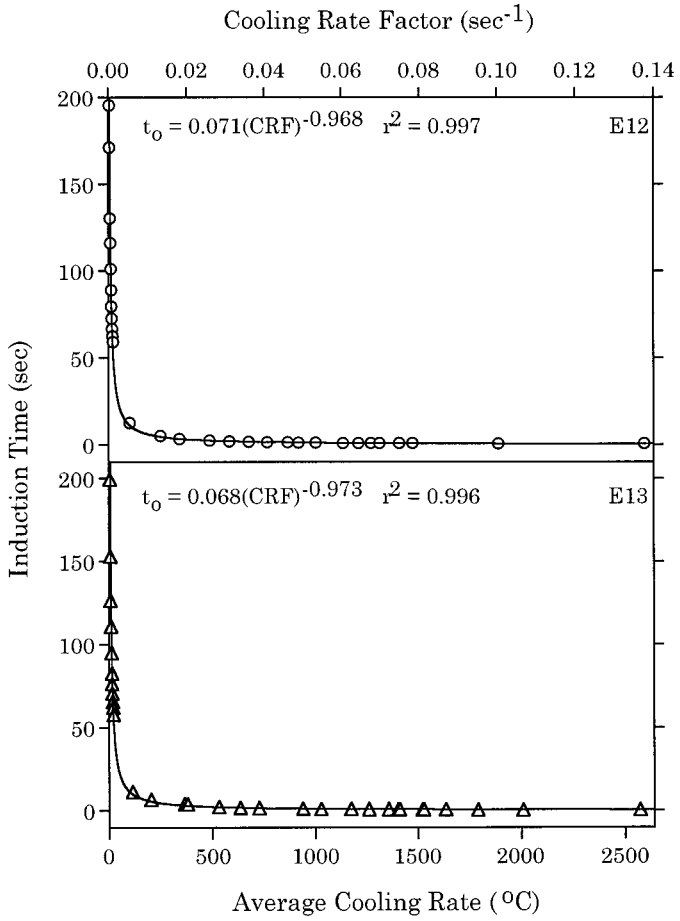

Figure 7. Induction time versus average cooling rate and/or CRF.

t_0, as a function of CRF and/or average cooling rate for each resin. The induction times follow a power law relationship with the value of CRF or average cooling rate as shown by the equations inset in Figure 7.

Crystallization half-times, defined as the time from the initiation of crystallization to the point where $\theta(t) = 0.5$, are plotted versus CRF and/or average cooling rate in Figure 8. The crystallization half-times also decrease rapidly with CRF for small values of CRF (< 0.005 s) and then decrease at a much slower rate as the half-times become very short. They also follow a power-law relation with CRF or average cooling rate as shown by the curves in Figure 8 and the inset equations.

The crystallization half-times are plotted against degree of supercooling, defined as the difference of the crystallization or plateau temperature from the relevant equilibrium melting temperature of each resin (Fig. 9a). This plot is one of the simplest ways to present the crystallization kinetics of the polymer. It should be noted here that since crystallization kinetics relates directly to the degree of supercooling rather than the crystallization temperature, use of the degree of supercooling is more favorable in this case where each resin has a different equilibrium melting temperature. The reciprocal half-times are also in use and are plotted against the crystallization temperature in Figure 9b. It can be interpreted from both Figure 9a and 9b that the E13 resin apparently crystallizes faster than E12 does, which corresponds well with the molecular weight effects observed in the growth studies described by Hoffman and Miller.[15]

Since a large fraction of the crystallization process takes place under pseudo-isothermal conditions, the Avrami-type analysis can be readily performed on the data collected. Recalling that the Avrami equation applies only after the incubation period, we may rewrite eq. (4) after taking double logarithms as

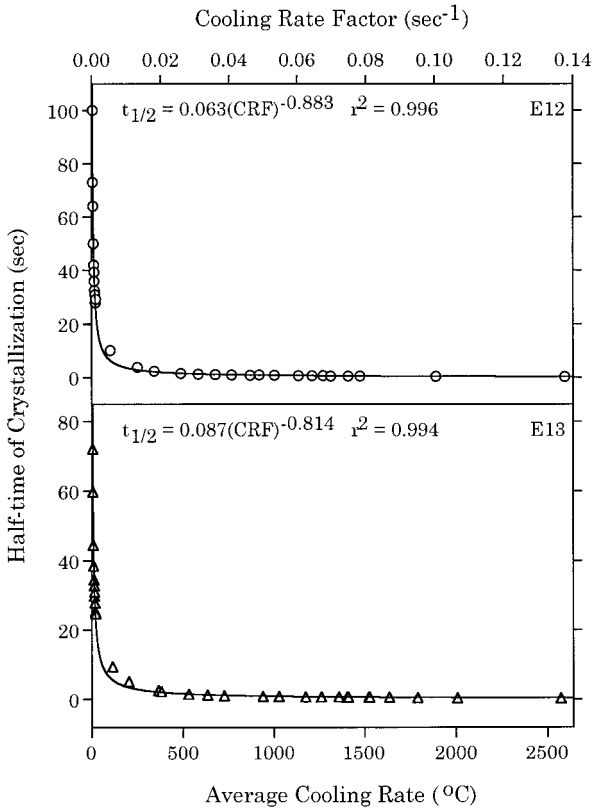

Figure 8. Half-time of crystallization versus average cooling rate and/or CRF.

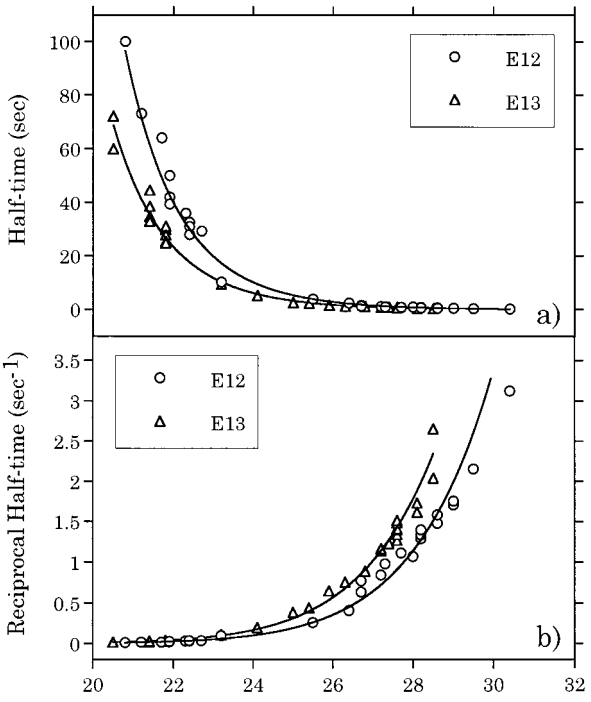

Figure 9. (a) Half-time of crystallization versus degree of supercooling. (b) Reciprocal half-time of crystallization versus degree of supercooling.

$$\ln\left\{\ln\left[\frac{1}{1-\theta(t-t_0)}\right]\right\} = \ln k + n\ln(t-t_0). \quad (8)$$

A plot of the left-hand side of eq. (8) versus $\ln(t - t_0)$ yields the Avrami exponent, n, from the slope and the rate constant, k, from the antilogarithm of the intercept. Figure 10 shows typical plots according to the above relationship for the E12 resin for five different cooling rates. It is easily seen that there is an inflexion point in each plot above which the secondary crystallization dominates the crystallization process.

Experimental results for the Avrami indices are presented as a function of CRF in Figure 11. It is clearly shown that the Avrami indices lie between 2.5 and 4. Even though, at very low CRF between 0.0002 to 0.0011 s, the Avrami exponents lie mostly between 3 to 4, compared to between 2.5 to 3 at larger CRF (0.0060–0.1376 s), it can be postulated with help from direct observation of spherulites in the microscope that the growth is three dimensional and the nucleation is predominently instantaneous. There does not appear to be a significant difference between the Avrami indices for the E12 and E13 resins. Thus, there is no significant difference in the Avrami exponents due to differences in molecular weight, at least for the two molecular weights studied.

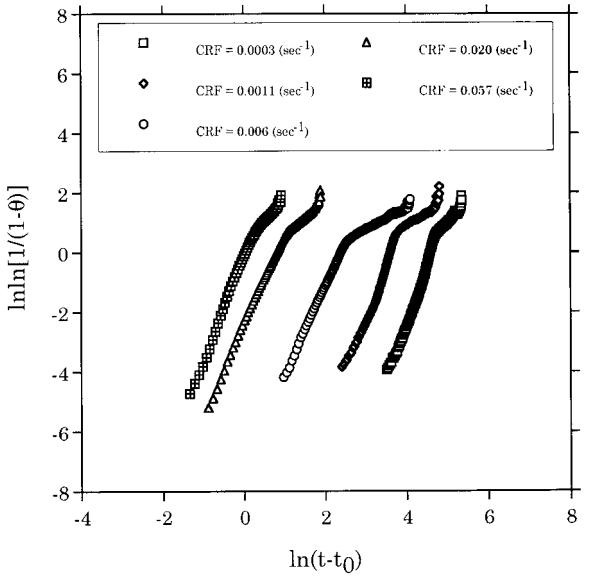

Figure 10. Typical plot of $\ln \ln[1/(1 - \theta)]$ against $\ln(t)$ for E12 resin at five cooling rates.

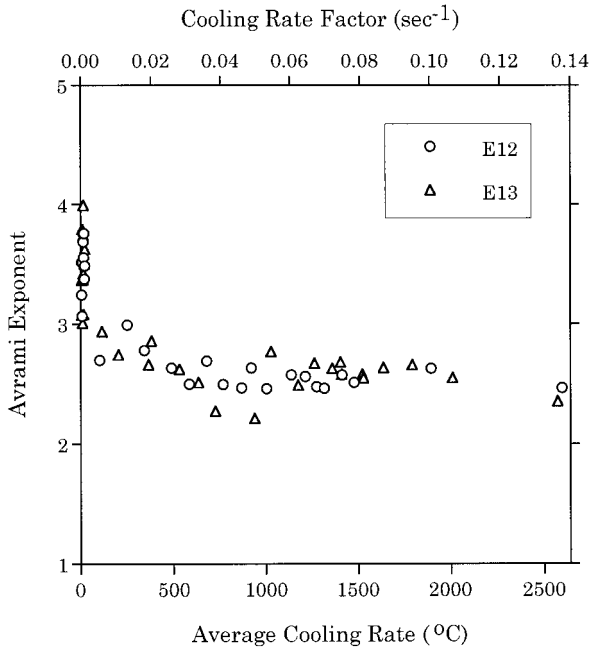

Figure 11. Avrami index versus average cooling rate and/or CRF.

Figures 12 and 13 illustrate the dependence of the crystallization rate constants on CRF and on plateau temperature, respectively. The values labeled "experimental" are obtained from the intercept of the Avrami plot while the values labeled "calculated" were obtained by use of the relationship:

$$k = (\ln 2)\left(\frac{1}{t_{1/2}}\right)^n, \qquad (9)$$

where $t_{1/2}$ is the measured crystallization half-time. The crystallization rate constants acquired from the plot were quite close to those calculated from eq. (9), which suggests that there was minimal error in the process of data collection and analysis. Both resins were found to crystallize faster as the cooling rate increases, and as the crystallization temperature decreases (degree of supercooling increases).

Crystallinity and Spherulite Size

It has often been suggested that the absolute crystallinity is a decreasing function of the cooling rate. This can be examined quantitatively for the present resins by measuring crystallinity of the samples prepared at different cooling rates. Two methods were used to measure the crystallinity: differential scanning calorimetry (DSC) and density gradient column (DGC). The results are shown in Tables I and II, respectively. The weight percent crystallinity was calculated based on the following equations:

$$\chi_c(\%) = \frac{\rho_c}{\rho}\left(\frac{\rho - \rho_a}{\rho_c - \rho_a}\right) \times 100, \qquad (10)$$

and

$$\chi_c(\%) = \frac{\Delta H_f}{\Delta H_f^o} \times 100, \qquad (11)$$

where ρ, ρ_a, and ρ_c are the sample density, and the density of the amorphous and crystalline regions, respectively, and ΔH_f and ΔH_f^o represent the enthalpy of fusion of the sample and of its 100% crystalline counterpart. The density values obtained from the literature[16] for linear polyethylene are $\rho_a = 0.855$ g/cm^3 and $\rho_c = 0.997$ g/cm^3. Two values of ΔH_f^o corresponding to different au-

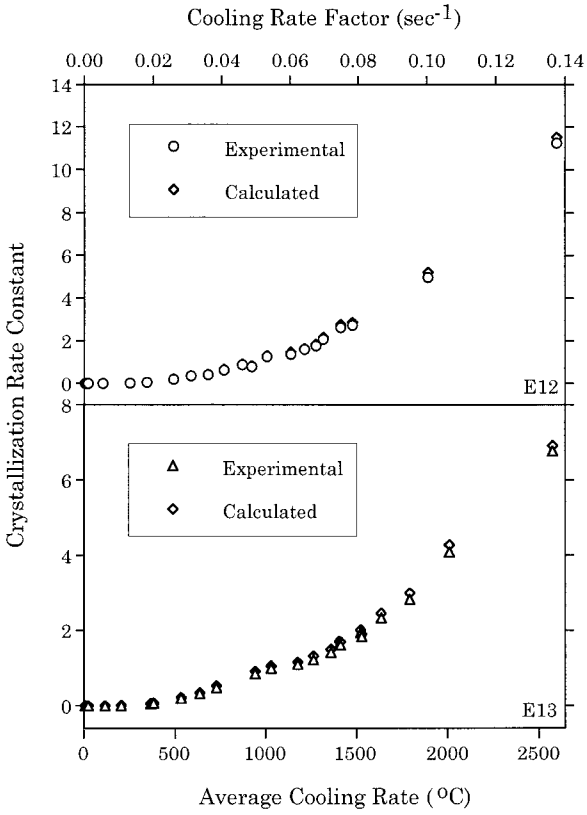

Figure 12. Crystallization rate constant versus average cooling rate and/or CRF.

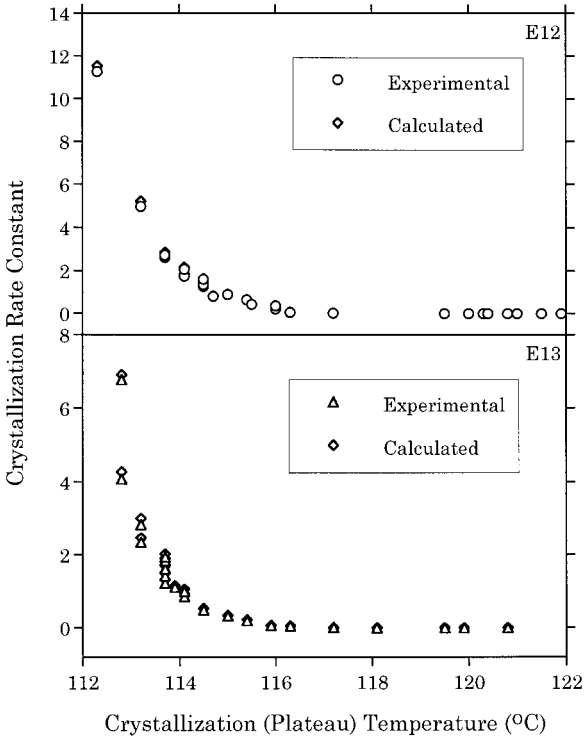

Figure 13. Crystallization rate constant versus crystallization temperature.

thors were used for comparison: $\Delta H_f^o = 276$ J/g[16] and $\Delta H_f^o = 288$ J/g.[17]

According to Table I, the melting peak temperature, the melting onset temperature, and the degree of crystallinity were all found to decrease with increase in average cooling rate. This corresponds well to the nature of the morphological picture of the polymer studied; lower crystallization temperatures would be expected to result in thinner lamellae. It is well known that the melting point of a given sample decreases with decrease of lamellar thickness.[18] Also at higher cooling rates, there is less secondary crystallization and, less annealing time for perfection of the lamellae formed. These effects result in the measurement of lower degrees of crystallinity at higher cooling rates from both DGC and DSC techniques. The differences of melting points and crystallinities between the two resins seem marginally significant.

According to Table II, the density data were found to lie roughly within the range 0.9380–0.9540 g/cm^3 for both resins. This is consistent with the density values supplied by the resin manufacturer of 0.9540 and 0.9512 for E12 and E13, respectively. Based on DGC data, the crystalline content varied from about 63% at high cooling rate to nearly 73% at very low cooling rate.

Glotin and Mandelkern[17] have investigated various HDPE fractions and found that crystallinity content calculated from density is always higher than that obtained from the heat of fusion due to contributions from the interfacial layer. This was found to be true here when the value of $\Delta H_f^o = 288$ J/g was used as shown in Tables I and II. However, when the value of $\Delta H_f^o = 276$ J/g was used, the calculated crystallinity content of E12 at low cooling rates was higher than that determined from the density. This illustrates the fact that the values of the parameters used are crucial to any comparisons made between crystallinity measurements determined from different techniques.

Small-angle light-scattering technique (SALS) was used to investigate the average spherulitic radius, R_{avg}, of the polyethylene samples, which were used for measurement of crystallinity. The results are also listed in Table II. The average spherulitic radii for both E12 and E13 resins were found to lie between 10 and 13 μm for the entire cooling rate range examined of 10–3500°C/min. Thus, there is little dependence of the spherulite size on the cooling rate. This further suggests that the nucleation density does not change appreciably with cooling rate. There are two possible ways for this to occur. Either (1) the ratio of growth rate to nucleation rate of the resins studied does not vary much or (2) nucleation occurs at a fixed number of predetermined sites. The latter seems more consistent with the crystallization kinetics results.

The Lauritzen and Hoffman Regime Analysis

The simplest method of presenting crystallization kinetics data is to plot the reciprocal of the half-time for the crystallization versus the degree of supercooling mentioned earlier and shown in Figure 9b. It should be mentioned once again that E13, which has lower average molecular weight than E12, crystallizes faster as expected.

According to the values of the Avrami index discussed previously, the crystallization kinetics of the resins studied were found to occur in the three-dimensional, instantaneous mode, which means the data should be analyzed by plotting $\log(t_{1/2})^{-1} + U^*/2.303R(T_c - T_\infty)$ against $1/T_c(\Delta T)f$. Parameters T_∞ and U^* are 160 K[19] and 6,276 J/mol,[11] respectively. The parameters T_m^o

Table I. Thermal Properties and Relevant Percent of Crystallinity

Resin	Sample Name	Average Cooling Rate (°C/min)	Melting Peak (°C)	Onset Temp. (°C)	ΔH_f (J/g)	Percent of Crystallinity	
						ΔH_f^o = 276 J/g	ΔH_f^o = 288 J/g
E12	SHS10	10.00	131.7	126.1	201.1	72.9	69.8
	SHS20	20.00	131.6	125.5	199.2	72.2	69.2
	SS000	67.86	130.6	125.4	194.7	70.5	67.6
	SS020	375.2	129.8	123.8	176.2	63.8	61.2
	SS040	794.2	129.4	123.6	172.9	62.6	60.0
	SS060	1060	129.1	123.5	170.0	61.6	59.0
	SS080	1133	129.0	123.3	168.1	60.9	58.4
	SS100	1585	129.0	123.3	163.1	59.1	56.6
	SS003	3251	128.7	123.0	161.4	58.5	56.0
	SS004	3535	128.6	122.8	160.8	58.3	55.8
E13	SHS10	10.00	131.7	124.7	191.0	69.2	66.3
	SHS20	20.00	131.3	124.0	189.3	68.6	65.7
	SS000	90.72	130.0	123.7	183.0	66.3	63.5
	SS020	449.8	128.2	122.1	181.0	65.6	62.8
	SS040	762.2	128.1	121.9	172.5	62.5	59.9
	SS060	1018	127.9	121.9	172.0	62.3	59.7
	SS080	1250	127.7	121.6	170.2	61.7	59.1
	SS100	1323	127.4	121.6	167.2	60.6	58.1
	SS003	2695	127.4	121.1	166.0	60.1	57.6
	SS004	3384	127.2	121.1	164.2	59.5	57.0

for E12 and E13 resins are 142.7 and 141.3°C, respectively. The modified Lauritzen-Hoffman plot for the data presented in Figure 9b is shown in Figure 14. With respect to the secondary nucleation theory by Hoffman et al.,[11] Figure 14 presumably shows regimes II and III. If this is the case, the shifts from regime II to III are found to be at 120.1 and 119.2°C for the E12 and E13 resins, respectively; this corresponds to supercoolings of 22.6 and 22.1°C, respectively. These experimental results correspond extremely well with the predicted regime II-III transition at supercooling of 23°C by Hoffman et al.[20]

Since the thermocouple used has an average standard error (according to the manufacturer's handbook) in the range of ±1 to ±1.5°C; transition temperatures would also have the same error limitation. Accordingly, the regime II–regime III transition temperature should be approximately 119 ± 1°C for both resins. According to Phillips and Lambert,[19] on cross-linked polyethylenes, they found that the regime II–regime III transition temperatures were 113°C for G-2.5 (molecular weight between cross-links of 1900) and 109°C for G-3.1 (molecular weight between cross-links of 1300), respectively. It seems that the regime II–regime III transition temperature of about 119°C as found in this work corresponds well with those found by these authors, considering that no cross-links exist in the present samples.

Let us consider the nucleation exponents, $K_{g,\mathrm{II}}$ and $K_{g,\mathrm{III}}$, which can be measured from the slope of the plot in Figure 14. Hoffman[21] found $K_{g,\mathrm{I}}$ and $K_{g,\mathrm{II}}$ to be 1.857×10^5 and 0.900×10^5 K^2; this result was obtained from growth rate data from various HDPE fractions. Phillips and Lambert[19] obtained $K_{g,\mathrm{I}}$ and $K_{g,\mathrm{II}}$ from the application of the half-time of the crystallization to the LH regime analysis to be 1.40×10^5 and 0.94×10^5 K^2, with the ratio of regime I–regime II slopes to be 1.49. In the present experiment, the average $K_{g,\mathrm{II}}$ and $K_{g,\mathrm{III}}$ for the original set of parameters, i.e., T_m^o(E12) = 142.7°C, T_m^o(E13) = 141.3°C, T_g = 190 K, U^* = 6276 J/mol, are 1.009×10^5 and 2.416×10^5 K^2, with the ratios of the regime III–regime II slopes being 2.44 and 2.28 for E12 and E13, respectively; compared with the theoretical value of 2.0.

In regimes I and II for HDPE obtained at low supercoolings, the ratios of $K_{g,\mathrm{I}}$ and $K_{g,\mathrm{II}}$ obtained from the growth data[11,15,20,21] are very close to the theoretical value of 2.0. In the analysis of the LH regime, secondary nucleation theory from bulk crystallization kinetics by use of half-time crystallization, however, it is not expected that the ratios of the regime III–regime II slopes equal 2.0. This

Table II. Density Data, Relevant Percent of Crystallinity, and Spherulitic Size

Resin	Sample Name	CRF (s)	Average Cooling Rate (°C/min)	Density (g/cm^3)	Percent of Crystallinity	R_{avg} (μm)
E12	SHS10	0.0006	10.00	0.9532	72.4	12.10
	SHS20	0.0011	20.00	0.9528	72.1	12.09
	SS000	0.004	67.86	0.9509	70.8	11.86
	SS020	0.020	375.2	0.9451	66.9	11.80
	SS040	0.043	794.2	0.9432	65.7	11.68
	SS060	0.055	1060	0.9421	64.9	11.59
	SS080	0.063	1133	0.9419	64.8	11.59
	SS100	0.089	1585	0.9413	64.4	11.55
	SS003	0.180	3251	0.9395	63.2	11.16
	SS004	0.192	3535	0.9386	62.5	11.04
E13	SHS10	0.0006	10.00	0.9535	72.5	12.72
	SHS20	0.0011	20.00	0.9513	71.1	12.13
	SS000	0.005	90.72	0.9495	69.9	11.66
	SS020	0.023	449.8	0.9441	66.3	11.44
	SS040	0.040	762.2	0.9440	66.2	11.34
	SS060	0.054	1018	0.9424	65.1	11.19
	SS080	0.068	1250	0.9424	65.1	11.16
	SS100	0.071	1323	0.9425	65.2	11.03
	SS003	0.148	2695	0.9404	63.8	10.71
	SS004	0.182	3384	0.9398	63.3	10.60

is partly because, as mentioned earlier, there are a number of processes involved in the bulk crystallization kinetics, such as the nucleation rates, the growth rates, secondary crystallization, and so on. Under these conditions, the values observed here of 2.44 and 2.28 for E12 and E13, respectively, seems reasonable.

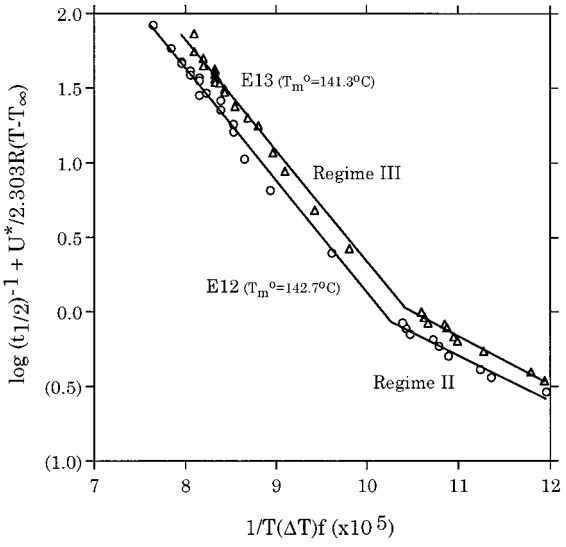

Figure 14. Resulting LH regime plot for E12 and E13 resins (spherulitic growth and instantaneous nucleation).

Recently, Fatou et al.[22] found that the regime II–regime III transition temperature increases with molecular weight. They found that the transition ranges from 119°C for $M_w = 1.95 \times 10^4$ to 120.5°C for $M_w = 8.0 \times 10^5$. In their analysis, the transport term was neglected, since HDPE crystallizes very rapidly and the crystallization temperature range is usually bound to the nucleation-controlled region, whereby plotting $\log(t_{1/2})^{-1}$ against $1/T_c(\Delta T)f$ is satisfactory enough to observe the regime behavior. We have also plotted our data in this way and found that the shifts of regime II to III occur at 120.0 and 119.2°C for E12 and E13, respectively; which are very close to those observed with the inclusion of the transport term. These values are very close to those found by Fatou et al. The ratios of the regime III–regime II slopes are found to be 2.43 and 2.26 for E12 and E13, respectively.

CONCLUSIONS

The present nonisothermal crystallization studies showed that, overall, bulk crystallization kinetics

are a strong function of the cooling rate. Within the range of cooling rates studied, increased cooling rate leads to decreasing crystallization temperatures and rapidly increasing crystallization rates. Despite the rapid cooling rates, the bulk of the crystallization takes place at a pseudo-isothermal temperature created by a balance between the rate of heat removal and the rate at which the heat of crystallization is evolved. The new technique used for these measurements gave quite reproducible, quantitative results under conditions that could not previously be studied.

The lower molecular weight resin crystallized slightly faster than the higher molecular weight resin for the whole range of the degree of supercoolings studied. This suggests that molecular mobility of the lower molecular weight linear polyethylene is greater than that of the higher one. During crystallization, the molecules can extricate themselves from the entangled melt much easier, resulting in less time required to complete the crystallization process.

The density data obtained from DGC exhibited a significant dependence on the cooling condition of the samples. A similar relation was also found with the degree of crystallinity data obtained from both DGC and DSC techniques. Both the density and the degree of crystallinity decreased with an increase in CRF and the degree of supercooling. These results are caused by changes in lamellae thickness and incorporated defects such as loose loops, dangling chain ends, higher degree of nonadjacent re-entry, etc.

Final spherulite radii measured by SALS did not vary much over the cooling rate and crystallization temperature range studied. This further suggests that the number of spherulites and, hence, the nucleation density did not change much with cooling rate or crystallization temperature. This result provides additional support for the conclusion deduced from the overall bulk crystallization kinetics that the growth geometry was spherical and the nucleation was instantaneous at predetermined sites.

Finally, the modified Lauritzen and Hoffman regime crystallization analysis exhibited a significant regime transition for both resins. It is believed that the transition that is observed is the regime II–III transition. The values obtained for the transition temperatures correspond quite well with the value predicted theoretically by Hoffman.[20] The transition temperatures were found to occur at roughly 119 ± 1°C and this corresponds to a supercooling of approximately 22 ± 1°C for both resins. The ratios of the regime III–regime II slopes were roughly 2.4 and 2.3 for E12 and E13, respectively; compared with the theoretical value of 2.0.

REFERENCES AND NOTES

1. S. Buckser and L. H. Tung, *J. Phys. Chem.,* **63,** 763 (1958).
2. L. Mandelkern, in *Growth and Perfection of Crystals,* R. H. Doremus, B. W. Roberts, and D. Turnbull, Eds., John Wiley & Sons, New York, 1958.
3. W. Banks, M. Gordon, R. J. Roe, and A. Sharples, *Polymer,* **4,** 61 (1963).
4. Y. K. Godovsky and G. L. Slonimsky, *J. Polym. Sci., Polym. Phys.,* **12,** 1053 (1974).
5. M. R. Kamal and E. Chu, *Polym. Eng. Sci.,* **23**(1), 27 (1983).
6. Z. Ding and J. E. Spruiell, *Soc. Plas. Eng. Tech. Papers* (*ANTEC*), **40,** 1485 (1994).
7. Z. Ding and J. E. Spruiell, *J. Polym. Sci., Polym. Phys.,* **34,** 2783 (1996).
8. J. H. Magill, *Polymer,* **2,** 221 (1961).
9. J. H. Magill, *Polymer,* **3,** 35 (1962).
10. M. Avrami, *J. Chem. Phys.,* **8,** 212 (1940).
11. J. D. Hoffman, G. T. Davis, and J. I. Lauritzen, in *Treatise on Solid State Chemistry,* vol. 3, N. B. Hanny, Ed., Plenum Press, New York, 1976.
12. A. Ziabicki, in *Fundamentals of Fibre Formation,* John Wiley & Sons, London, 1976, p. 173.
13. J. R. Dees and J. E. Spruiell, *J. Appl. Polym. Sci.,* **18,** 1053 (1974).
14. M. Kim, in Ph.D. dissertation, University of Tennessee at Knoxville, 1996.
15. J. D. Hoffman and R. L. Miller, *Macromolecules,* **21,** 3038 (1988).
16. J. Brandup and E. H. Immergut, in *Polymer Handbook,* John Wiley & Sons, New York, 1966.
17. M. Glotin and L. Mandelkern, *Colloid Polym. Sci.,* **260,** 182 (1982).
18. B. Wunderlich, in *Macromolecular Physics,* vol. 2, Academic Press, New York, 1976.
19. P. J. Phillips and W. S. Lambert, *Macromolecules,* **23,** 2075 (1990).
20. J. D. Hoffman, *Polymer,* **24,** 3 (1983).
21. J. D. Hoffman, *Polymer,* **23,** 656 (1982).
22. J. G. Fatou, C. Marco, and L. Mandelkern, *Polymer,* **31,** 1685 (1990).